Department of Physics and Astronomy
University of Heidelberg

Bachelor Thesis in Physics
submitted by

Jan Horak

born in Paderborn (Germany)

2017

Mono-X Collider Searches for Dark Matter

This Bachelor's Thesis has been carried out by Jan Horak at the
Institute for Theoretical Physics in Heidelberg
under the supervision of
Prof. Dr. Tilman Plehn

Abstract

We study mono-X signatures of Dark Matter (DM) pair production at the Large Hadron Collider (LHC) at collision energies of $\sqrt{s} = 13$ TeV and a luminosity of $\mathcal{L} = 10$ fb^{-1}. These signals arise in the form of a particle X plus missing transverse energy. We focus on X to be a jet, photon or Z-boson. For the mono-Z channel, we consider a leptonic decay into a $\mu^+\mu^-$-pair. The dark sector is modelled using a simplified model approach, coupling a complex scalar DM agent to the Standard Model through a 1 TeV dark vector mediator. In this scenario, signals only arise from initial state radiation (ISR). The LHC sensitivity to these signatures is tested and the kinematic details of all processes are examined and presented. We find similar behaviour for the mono-jet and mono-photon channels and deviating structures for the mono-Z channel due to the high Z mass. Mono-jet signatures clearly give the highest sensitivity, disfavouring mono-photon and mono-Z searches in ISR model frameworks.

Wir untersuchen Mono-X Signaturen aus Dunkle Materie (DM) Paarproduktion am Large Hadron Collider (LHC) bei Kollisionsenergien von $\sqrt{s} = 13$ TeV und einer Luminosität von $\mathcal{L} = 10^{-1}$. Diese Signale treten als Teilchen X zusammen mit fehlender transversaler Energie auf. Wir betrachten X in Form von Jets, Photonen und Z-Bosonen. Im Mono-Z Kanal wird ein leptonischer Zerfall in ein $\mu^+\mu^-$-Paar angenommen. Der DM Sektor wird mithilfe eines *simplified model* Ansatzes modelliert, indem wir ein komplexen DM Skalar an das Standardmodel durch ein 1 TeV dunkles Vektorboson koppeln. In diesem Szenario treten Signale nur aus *initial state radiation* (ISR) auf. Wir testen die LHC Sensitivität auf diese Signaturen und untersuchen die kinematischen Details der Streuprozesse. Zwischen dem Mono-Jet und Mono-Photon Kanal stellen wir ähnliches Verhalten fest. Für die Mono-Z-Signatur finden wir Abweichungen aufgrund der hohen Z-Masse. Der Mono-Jet Kanal liefert die deutlich höchste Sensitivität und zeigt somit klare Vorteile gegenüber Mono-Photon und Mono-Z Suchen im Rahmen von ISR Modellen.

Contents

List of Figures

List of Tables

1 Introduction

Measurements of galaxy rotation curves show data that, in the framework of general relativity, cannot be fitted to the visible amount of matter observed in the centre of the galaxies. This implies that either our understanding of gravity at cosmological scales is wrong or an additional form of matter, which is invisible to us, has to exist. A way to account for this additional matter is called Dark Matter (DM). It introduces new particles that are not yet detected. Assuming that these particles explain the phenomenon of additional matter, cosmological observations show that DM makes up $\frac{5}{6}$ of all matter in our Universe.

While galaxy rotation curves represent the most historic hint for DM, there are several more recent signs of DM, which allow us to learn more about this unknown form of matter. An often discussed observation hinting DM are temperature fluctuations in the cosmic microwave background (CMB). This will be explained in the following section. However, these two phenomenons are not the only signs of DM that have been found so far. More hints on the existence of DM can be observed for example in gravitational lensing or structure formation.

1.1 The CMB

A strong hint for DM can be found the CMB, shown in Fig. 1.1. The CMB is a uniform background black body radiation coming from all directions in the sky. It consists of photons with wavelengths in the microwave range that stream freely across the entire cosmos. In that sense, as a relic from when our Universe was still in its early stages, the CMB spectrum contains a lot of valuable data about the Universe's origin. A look at the heat map of the CMB shows a nearly homogeneous temperature distribution averaging at around 2.725 K [1]. However, small fluctuations of the order of 10^{-4} K can be observed in the spectrum. The reason for these anisotropies is nontrivial. In the early Universe, all of today's matter was contained in a very dense and uniform plasma, called photon-baryon fluid. By expansion of the Universe, the fluid cooled down and allowed the contained particles to combine and form today's matter. Assuming a homogeneous energy distribution inside this plasma, which contained also today's CMB

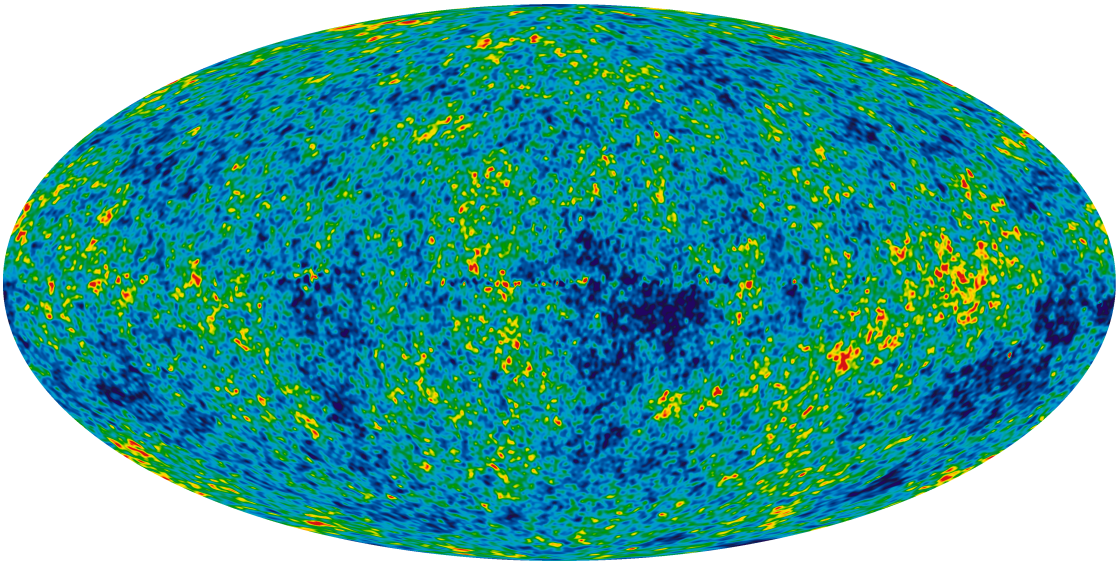

FIG. 1.1: Heat map of the CMB observed by the satellite WMAP. Red corresponds to higher and blue to lower temperatures. Picture taken from [1].

photons, there should not arise inhomogeneities in the CMB spectrum. One of the phenomena being responsible for the nevertheless existing anisotropies are so-called baryonic acoustic oscillations. It is assumed, that the dark sector decoupled much earlier from the photon-baryon fluid than the CMB photons. The decoupled DM self-interacts gravitationally and, by quantum fluctuations, clumps together, hence forming gravitational wells. These gravitational wells pull against the radiation pressure inside the wells, leading to oscillations. The oscillations cause frequency differences within the at that point decoupling photons, that now form the CMB. These deviating frequencies are observed in the CMB, making another strong argument for DM.

In many theories, particle physics approaches to the nature of DM have been worked out. In these, new particles, that are not included in the Standard Model (SM), are introduced to account for these anomalies. A common assumption is for DM to be a weakly interacting massive particle (WIMP). Also contrary approaches, where DM is an ultra light particle called axion, have been worked out. To test these models, different kinds of experiments were developed which search for these yet undiscovered particles. In the following, a short introduction to the so-called WIMP miracle will be given to motivate later assumptions on the nature of the DM particle.

1.2 WIMP Miracle

We learned earlier, that DM makes up about $\frac{5}{6}$ of the matter content in our Universe. Commonly, the DM content is given in form of a dimensionless parameter

$$\Omega_\chi = \frac{\rho_\chi}{\rho_c} \ , \tag{1.1}$$

called relic density. ρ_χ is the DM density of today in the Universe and ρ_c is the critical density, defined by the matter density of a flat Universe, separating an expanding from a collapsing Universe. The actual matter density in the Universe is in fact measured to almost perfectly agree with ρ_C. From CMB fluctuations for example, the relic density is measured to

$$\Omega_\chi h^2 = 0.1198 \pm 0.0015$$

with h being the Planck constant [2]. Introducing new particles to account for the observed phenomena, theories always have to be tested against this measurement. The WIMP model assumes the DM candidates to be massive and weakly interacting with the SM. Due to the high mass, the WIMPs are assumed to be non-relativistic when decoupling from the thermal equilibrium with the photon-baryon fluid. This feature makes the model also agree with observation from large scale structure formation, requiring DM to be sufficiently cold to form today's structure of the Universe. Based on the assumptions of the WIMP hypothesis, one can compute the relic density as a function of the DM mass m_χ, and finds

$$\Omega_\chi h^2 \approx 0.12 \left(\frac{150 \text{ GeV}}{m_\chi} \right)^2 \ . \tag{1.2}$$

Thus, for a particle of about 150 GeV, the relic density comes out exactly right [3]. This is referred to as the WIMP miracle and motivates assuming a DM mass in the GeV-TeV range, which we will also do in our model.

In chapter 2, a short introduction to the experimental searches for DM will be given, including the relevant collider kinematics background. This will be followed up by the theoretical framework in terms of particle physics we used to describe DM, in chapter 3. After that, in chapter 4, the results of our collider simulations will be presented. To conclude, we will discuss the obtained results and give an outlook to future research chances.

2 Experimental Searches for Dark Matter

The main challenge in searching for possible DM agents is already implied in the name Dark Matter itself. The reason we have not seen it so far is the lack of (observable) interaction. The searches for particle DM are hence based on the assumption that there is a non-vanishing interaction, which couples DM to the SM. Commonly, DM search experiments are categorized into three different types. While the focus of this work will lie on the collider search done at the LHC, also the other two experimental approaches, called direct and indirect detection, will briefly be sketched. A short overview of the underlying, complementary strategies of these two will be given, before moving on to collider searches.

2.1 Direct and Indirect Detection

Direct detection experiments are usually designed to detect DM in the WIMP mass range between 10 and 400 GeV. It is aimed to observe the direct recoil of a nucleus hit by a possible DM particle. To get a maximal recoil energy, it is of advantage to use nuclei with a mass similar to the mass the DM particle is expected to have. Since the DM-SM interaction is assumed to be extremely small, these experiments need to have a very high sensitivity in order to not miss any possible collision between DM and the target nuclei. Therefore, the experiment needs to be set up somewhere, where the solar and cosmic background radiation is as small as possible. Also, a large amount of target material makes it more likely to detect an event, assuming a non-vanishing interaction. A common way to achieve high sensitivity is by installing the experiment deeply underground with large containers filled with relatively heavy nuclei as target material. This is done for example at the XENON Dark Matter Project at the Italian Gran Sasso Laboratory [4]. In this experiment it is aimed to observe elastic scattering of DM off Xe nuclei.

The results obtained in direct detection experiments so far put strong exclusion limits on the coupling between DM and the SM. However, so far direct detection experiments

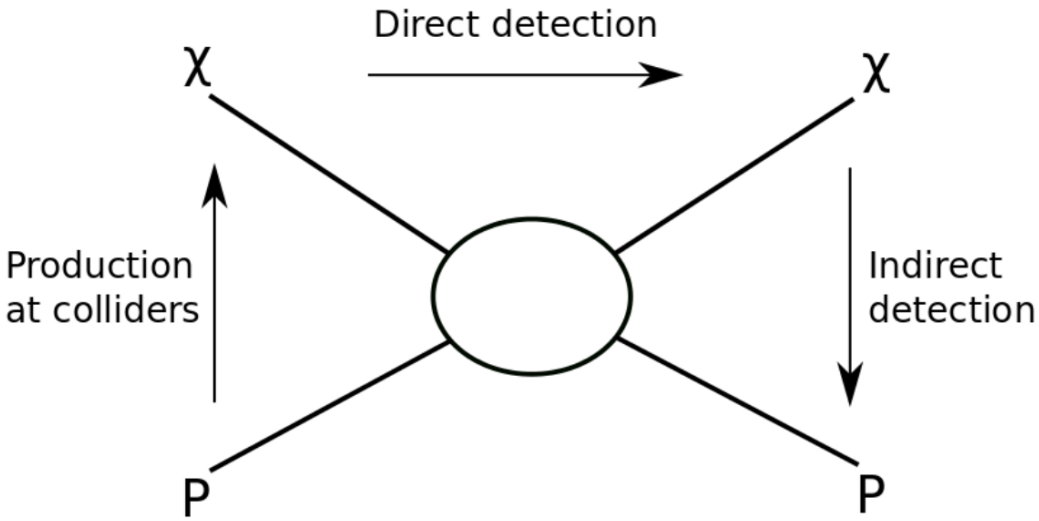

FIG. 2.1: Schematic overview of DM search channels. χ is a DM particle, P is a proton. The middle circle represents an interaction between the particles connected by the lines. The arrows are pointing from the initial state particles to the final state particles. [5]

are limited in their precision by neutrino and other type of background.

The strategy behind indirect DM searches is a different one. Here, experiments search for a DM-DM-annihilation into ordinary matter. Due to the observed gravitational interaction of DM, it is assumed to clump wherever there are big sources of gravity, such as stars or black holes. Thus, in these regions, a significantly enhanced annihilation rate is expected. Then, possible decay products, such as neutrinos or photons, of these self-interactions could be observed. As an example, the Fermi Large Area Telescope is designed to detect gamma-rays from DM-DM-annihilations. However, since not only DM is clumping around massive objects, there are also a lot of other interactions happening in these regions. The background radiation is hard to estimate due to large theoretical uncertainties. This makes it a tough cosmological challenge to filter for a clear signal from DM-pair-annihilation. [3]

2.2 Collider Searches

In collider searches, one tries to produce DM in SM particle collisions (see Fig. 2.1). The production rates of DM particles in particle collisions scale with the collision energy $\sqrt{s}$. Therefore, as the LHC reaches higher and higher energies, collider searches for DM

are increasingly drawing attention. Due to the previously unmatched scales, missing transverse energy ($\not{E}_T$) signatures represent a promising way to look for new physics, extending the SM. Events like $pp \to X + \not{E}_T$ can hint the existence of DM in form of a particle. The focus of this work will particularly lie on X to be a photon, jet or Z-boson, which will be referred to as mono-photon, -jet or -Z signals.

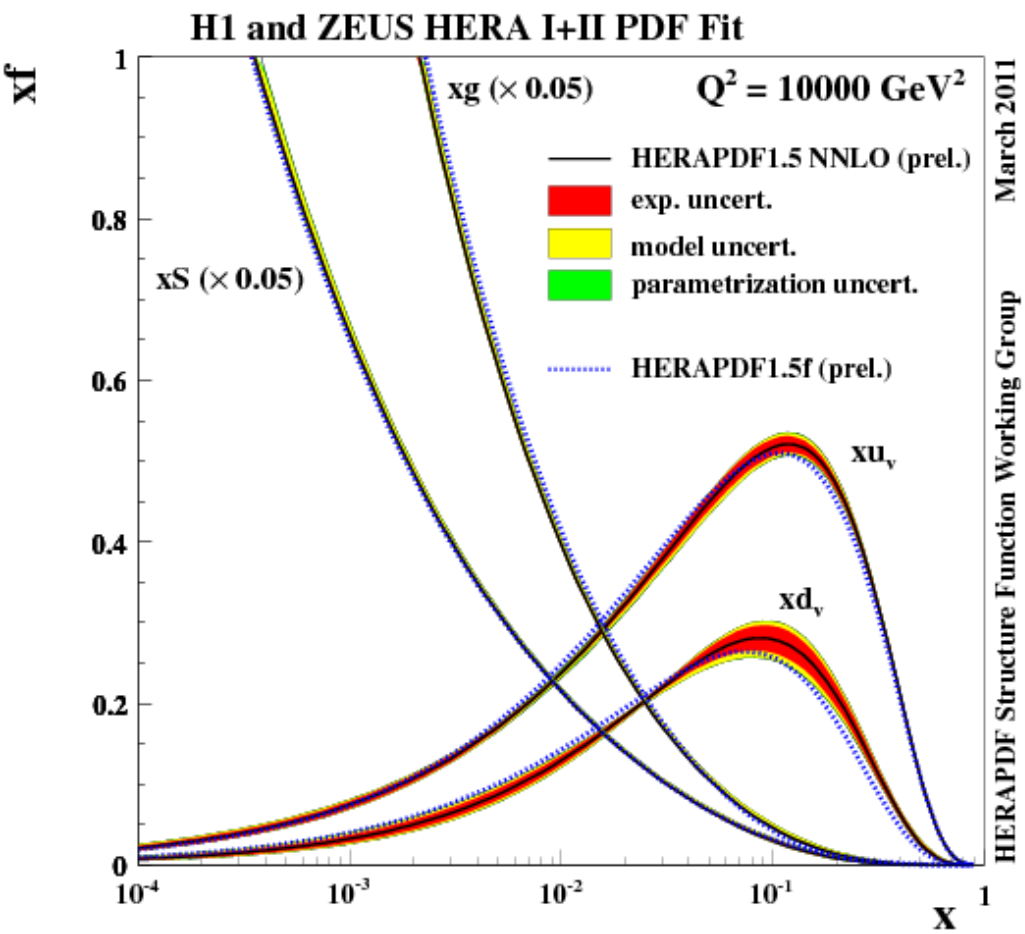

FIG. 2.2: Parton density functions (pdfs) of the proton measured by HERA. The gluon and sea quark pdfs are scaled down by a factor of 20. [6]

At hadron colliders, it has to be taken into account that as a result of the particles being very energetic, the colliding hadrons get resolved into their very constituents, called partons. Therefore, the actual scattering processes are happening on parton level. However, the exact energies of the quarks inside an incoming proton are unknown. Hence, there is a lack of knowledge about the partons' initial momenta, especially in

the longitudinal direction, which is relevant for the scattering. In order to compute cross-sections, we need information about the longitudinal boosts from the hadron's rest into the partons' centre of mass frame. In particular, we are looking for the fractions x of the hadron momentum that is carried by each of the partons taking part in the interaction. These fractions are given by the energy-dependent inner structure of the hadrons, which is described by the parton density function (pdf) $f_i(x)$ (see Fig.2.2). It gives the probability of the parton i to carry the fraction x of the total hadron momentum.

Using these variables, we can express the hadronic cross-section of DM-pair-production in a proton-proton-collision (assuming only quark-anti-quark initial states) as

$$\sigma(pp \to \chi\chi) = \int_0^1 dx_1 \int_0^1 dx_2 f_q(x_1) f_{\bar{q}}(x_2) \sigma_{q\bar{q}\to\chi\chi}(x_1 x_2 S) \ , \tag{2.1}$$

with S being the hadron collision energy and the partonic cross-section $\sigma_{q\bar{q}\to\chi\chi}$. The incoming colliding particles are travelling in the positive and negative z-direction. Thus, by momentum conservation, in the final state one expects

$$\sum_{\text{final state j}} \vec{p}_{T,j} = 0 \ , \tag{2.2}$$

with $\vec{p}_T$ being the projection of the momentum onto the transverse plane, called transverse momentum. Longitudinally, the momentum can be parametrized through a boost from the hadron center of mass (CM) frame. This is done using the rapidity y, defined through

$$\begin{pmatrix} E \\ p_L \end{pmatrix} = m \begin{pmatrix} \cosh y \\ \sinh y \end{pmatrix} \ , \tag{2.3}$$

where p_L is the longitudinal momentum, m the invariant mass and E the total energy. Rewriting Eq. (2.3), we find

$$\frac{1}{2} \log \frac{E + p_L}{E - p_L} = y \ . \tag{2.4}$$

It can be easily checked that y is additive. For massless or highly relativistic particles, we can assume $E = |\vec{p}|$. This gives

$$y = \frac{1}{2} \log \frac{|\vec{p}| + p_L}{|\vec{p}| - p_L} = \frac{1}{2} \log \frac{1 + \cos\theta}{1 - \cos\theta} = -\log \tan \frac{\theta}{2} \equiv \eta \ , \tag{2.5}$$

where θ is the polar angle and η is called pseudorapidity. Using this, the longitudinal

momentum of final state particles can be determined. Also taking into account the azimuthal angle Φ, under which the final state particle is propagating, the particles' momenta are fully parametrized.

Using momentum conservation, after the collision process, Eq. (2.2) is expected to hold. However, this is not always the case. Possible reasons for this are invisible[1] particles in the final state, like our DM particles. This is referred to as missing transverse momentum ($\vec{\not{p}}_T$). We call the modulus $|\vec{\not{p}}_T| = \not{E}_T$ missing transverse energy. Processes with invisible final state particles appear in the SM as well, for example with outgoing neutrinos. The cross-sections of the SM processes, however, are known. Hence, we can interpret deviations from the SM expectations as signals coming from DM. For this reason, missing transverse momentum represents a key observable in DM searches at colliders. Another import experimental quantity is the rapidity y introduced in Eq. (2.4). As it is related to the longitudinal boost of the final state particles from the hadron CM frame, we can deduce additional kinematic information about our processes. For massless particles for instance, y coincides with the pseudorapidity η introduced in Eq. (2.5). In that case, we can deduce direct information about the angular scattering spectrum from y. [7]

[1] In this sense, invisible means invisible to the detector. As the detector does not register invisible particles (and in particular their momenta), by momentum conservation, the final transverse momenta (in most of the cases) do not add up to zero.

3 Simplified Model Approach to Mono-X Signatures

In this chapter, our choice of model describing the dark sector will be introduced. This model will later be used to run simulations that make predictions for signals at the LHC.

To describe the interactions between the dark sector and the SM, which lead to signals at the LHC, an appropriate theoretical framework is needed. We decided for an approach called simplified model. Simplified models are used to describe new physics, introducing a controllable set of parameters such as masses and couplings of the new particles. With these scenarios, it is easy to test for collider sensitivity to the new parameters, without being too explicit about details and consequences of the theory that are not of interest for the observations. A simplified model is realized through an effective Lagrangian, describing the relevant interaction. In this way, also the kinematics of possible mediators can be studied, in dependence of the model parameters. [8]

Using this approach, we model a DM pair production mechanism through a new heavy vector boson Z' decaying into a DM particle pair $Z' \to \chi\chi$. The Z' boson arises as mediator particle of a new gauge group $U(1)'$. For simplicity, Z' on the SM side is only coupled to quarks, since this is sufficient for our studies. Assuming χ to be a complex scalar, the DM part of the Lagrangian can be written

$$\mathscr{L} \supset g_q \bar{q}\gamma^\mu(1+\gamma_5)qZ'_\mu - ig_\chi\{\chi^\dagger\partial^\mu\chi + \chi\partial^\mu\chi^\dagger\}Z'_\mu + g_\chi^2|\chi|^2 Z'_\mu Z'^\mu. \tag{3.1}$$

Looking at Eq. (3.1) tells us, that possible mono-X signals can only be radiated off the incoming initial state particles. Z' cannot radiate any single jets or photons. Further, χ

Couplings		Masses	
g_q	g_χ	$m_{Z'}$ [GeV]	m_χ [GeV]
0.25	1	1000	10

TABLE 3.1: Parameter choice of the simplified model for a complex scalar DM.

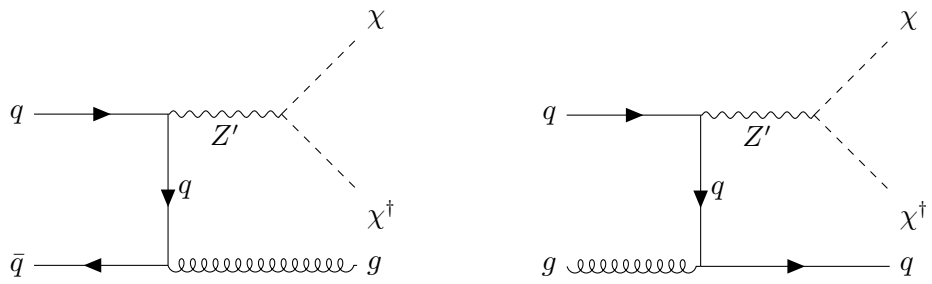

FIG. 3.1: Feynman diagrams of the mono-jet signatures from DM-pair-production. Left: Quark and anti-quark in the initial state. A gluon is radiated as jet. Right: A quark and a gluon in the initial state. The jet is a quark

only interacts through the mediator. It becomes clear that by gauge invariance, χ can only be produced in pairs, if it is charged under $U(1)'$.

The Feynman diagrams of a mono-jet signal are shown in Fig. 3.1. Similarly, we can also get a photon or a Z instead of the jet in the final state of the left diagram.

At this point it can already be seen, that $m_{Z'}$ is a crucial parameter for this model, as it suppresses the production rates through the propagator as long as Z' is heavy compared to the average parton CM energy. In this case, the exact choice for m_χ is not of importance, as long as $m_\chi \ll m_{Z'}$ holds. Furthermore, comparing only signals within this model, also the choice of the SM coupling g_q of Z' does not play a role for the relative signal strengths. However, to make exact predictions of the LHC sensitivity, the signatures have to be compared against their respective background. As in this case absolute rates become important, the exact choice of the couplings has to be carefully taken care of.

4 Collider Sensitivity

By setting up the required theory for the dark sector, the groundwork for exploring the kinematic features of the model and estimating LHC sensitivities for the different signatures is laid. To compute sensitivities, it is necessary to consider the background that occurs in experiments. Since the observed signals from the DM-pair-production will be of the form $X + \not{E}_T$, the irreducible background needs to have invisible final state particles in order to give the same signature. We model it by $pp \to \nu\bar{\nu} + X$ with a SM Z in the intermediate state. Reducible background is not taken into account. X is considered to be a single jet, photon or Z decaying into a $\mu^+\mu^-$-pair. The muon decay channel has little SM background and is thus easy to detect. Due to the high mass of the Z, compared to the photon, we expect much smaller rates. Further, by the difference in coupling strength, we expect mono-jet to have an advantage over mono-photon and mono-Z. The DM model Lagrangian form Eq. (3.1) is implemented using FEYNRULES [9]. For each process, $N = 10^6$ events are generated at leading order with a collision energy of $\sqrt{s} = 13$ TeV using Monte Carlo simulation with MADGRAPH [10]. During event generation, for technical reasons a cut of $p_T > 10$ GeV is applied to jets, photons and charged leptons. The total event rates are normalized to an integrated luminosity of $\mathcal{L} = 10$ fb^{-1}. MADANALYSIS [11] is used to analyze the MADGRAPH output.

The kinematic analysis will include looking at the missing transverse momenta and rapidities of the processes. For jets and photons, y is directly related to the scattering angle θ (see Eq. (2.5)). For a massive particle like the Z boson, we can only deduce informations about the longitudinal boost from the detector rest frame by y. Due to symmetry in the transverse plane, we will only look at $y > 0$. With the total number of signal and background events S and B, the significance R can be computed using

$$R = \frac{S}{\sqrt{B}} \ , \tag{4.1}$$

which represents a measure for the collider sensitivity with respect to a given signal and background.

mono	$\sigma_{pp\to\chi\chi^\dagger+X}$ [pb]	$\sigma_{pp\to\nu\bar{\nu}+X}$ [pb]	R
j	5.637 ± 0.001	4501 ± 2	8.402 ± 0.004
γ	$(9.298 \pm 0.003) \cdot 10^{-2}$	21.18 ± 0.01	2.020 ± 0.001
Z	$(1.703 \pm 0.001) \cdot 10^{-4}$	0.1149 ± 0.0001	$(5.402 \pm 0.001) \cdot 10^{-2}$

TABLE 4.1: Signal and background leading order production cross-sections of mono-jet, -photon and -Z signatures for a complex scalar DM agent at $\sqrt{s} = 13$ TeV. The computations were done based on a simulation with N=10^6 events. All uncertainties are of theoretical nature.

4.1 Final State Parton Level Analysis

The analysis is started on parton level, looking at the bare processes. Table 4.1 shows the signal and background production rate cross-sections and the significances for the analyzed processes. The jet cross-section is by far the biggest, while σ_Z at the order of 10^{-4} pb is extremely small. The significances confirm what can be see from the cross-sections. For a luminosity of $\mathcal{L} = 10$ fb^{-1}, we find that on parton level, the LHC is most sensitive to the mono-jet channel. The mono-photon significance is smaller by a factor of four, while the mono-Z significance lies below by two orders of magnitude. It becomes clear, that in this scenario, mono-Z searches are not very promising. Nevertheless, an analysis on the mono-Z channel will be conducted in order to understand the structure of this process.

The parton level p_T-distributions for the mono-jet, -photon and -Z channel can be seen in Fig. 4.1. Due to the bigger cross-section, the jet signal and background rates are higher than the mono-photon rates by about two orders of magnitude. The mono-Z rates lie below by several orders of magnitude. In addition to the event generation cuts, the same cut of $p_T > 10$ GeV is applied to the reconstructed Z in order to have comparable results.

The signal and background curves for mono-jet as well as mono-photon approach each other for higher p_T as can be seen on the top left of Fig. 4.1. The shapes of these four curves are very similar (see top right panel of Fig. 4.1). The curves are normalized to the total cross-section. The normalized mono-photon rates are higher than the mono-jet rates for very low p_T. The jets tend to be slightly harder[1]. As shown in the bottom left panel, in the y regime, jet and photon signals as well have a very similar shape .

The mono-Z rates are suppressed by the high Z mass. This is also the reason for the mono-Z signal and background curves to not monotonously decrease but to have a dip

[1]In the context of colliders, a hard signal consists of particles with large momentum, while a soft signal corresponds to particles with low momentum.

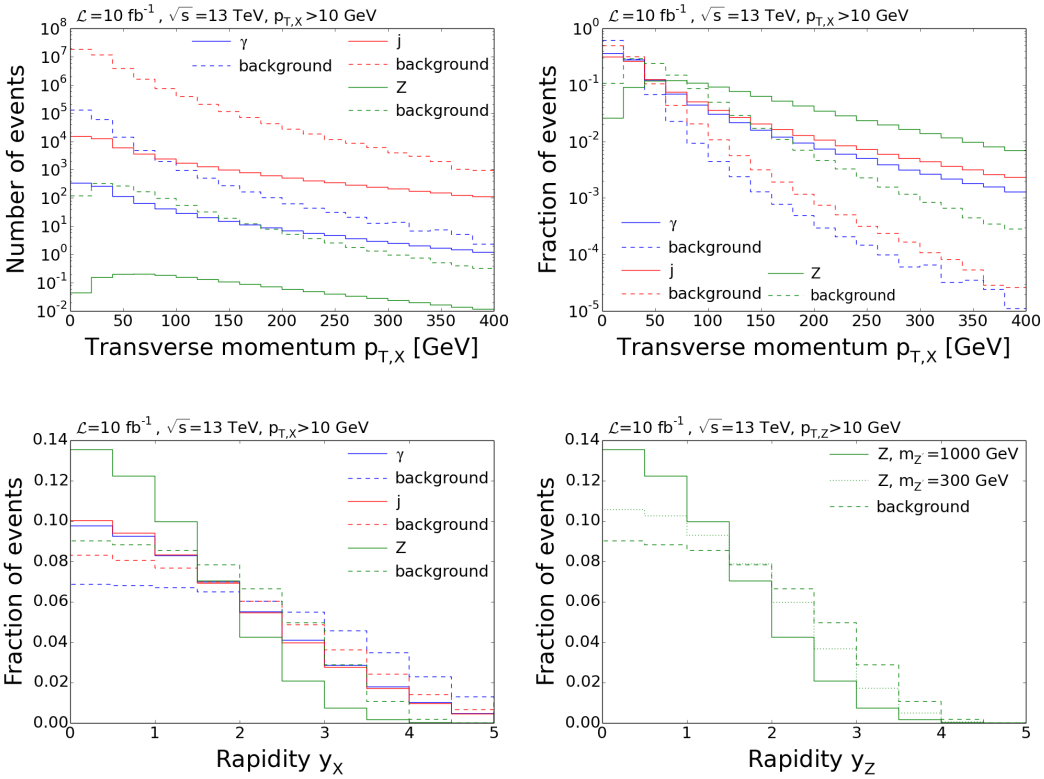

FIG. 4.1: Partonic mono-photon, -Z and -jet events over respective background. Top left: p_T-distributions of the total rates of all channels at $\mathcal{L} = 10$ fb^{-1}. Top right: p_T-distributions of all channels normalized to one. Bottom left: y-distributions of all channels normalized to one. Bottom right: y-distribution of the mono-Z channel with $m_{Z'} = 1000$ TeV and $m_{Z'} = 300$ TeV.

for very low p_T. Because for a Z on-shell production about 90 GeV are need, the final state particle is unlikely to have small transverse momentum. This argument will be explained in a more detailed way in the following.

The normalized p_T-distributions on the top right panel of Fig. 4.1 show, that all signals are significantly harder than their respective background. This can be explained looking at the normalized pdfs of the initial state particles at the on-shell production scales of the respective mediators (see Fig. 2.2). At the Z' on-shell production scale of about 1 TeV, it is more likely to produce particles with high momenta than at the Z on-shell production scale of 100 GeV. Hence, the signals are more likely to have high transverse momentum.

Another mass effect can be seen comparing all three channels normalized y-distribution on the bottom left of Fig. 4.1. The mono-Z signature is steeper than the mono-jet and mono-photon channel in signal and background as well. This shows that the Z-bosons

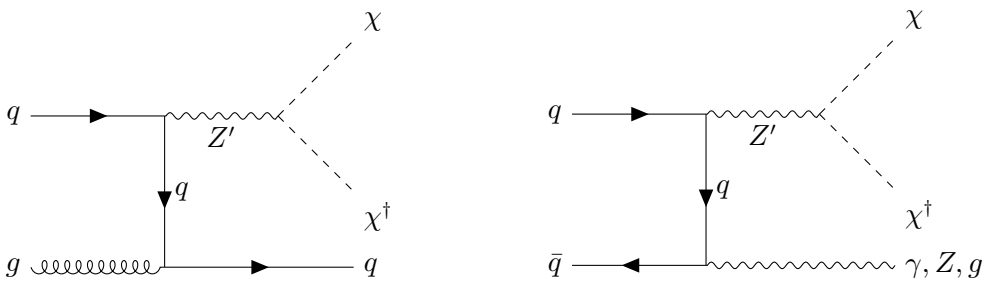

FIG. 4.2: Left: Parton level Feynman diagram of a mono-jet process with a quark-gluon initial state. Right: Parton level Feynman diagram of a mono-photon/Z process. We cannot have a gluon in the initial state, like on the left.

in the final state are more likely to be less boosted than the jets and the photons. When a Z is radiated off a quark, there is a minimal scattering angle as a result of the large Z mass. The mass forbids completely collineary radiation. Hence, the Z tends to have a smaller rapidity. The deviations between the mono-Z and signal's and background's y-distributions on the two bottom panels can as well be explained looking at the pdfs of the initial state particles. At $m_Z \approx 90$ GeV, the initial state q carries most of the energy, leading to a strong boost of the partons' centre of mass system (CMS). Thus, the background tends to have a higher rapidity. At $m_{Z'} = 1$ TeV, the energy distribution between the initial state particles is rather balanced. The parton CM frame is not strongly boosted as before. It can be seen, that the mono-Z signal distribution counts more events with little y.

The influence of $m_{Z'}$ on the signal's angular spectrum is shown on the bottom right of Fig. 4.1. With $m_{Z'} = 300$ GeV, the signal is boosted more, as the energy distribution between in the $q\bar{q}$ initial state is less balanced. The signal curve moves towards the background, as the signal and background mediator masses approach each other.

4.1.1 Reduced Mono-Jet

The bare mono-jet process is structurally different from the mono-photon and mono-Z process. The mono-jet has an additional quark-gluon initial state on top of the $q\bar{q}$ initial state. In the former case, the radiated jet will consist of a quark. This is not possible for mono-photon and -Z processes, where the incoming particles always are quarks, as illustrated in Fig. 4.2. To eliminate this channel from the mono-jet signal in order to make the processes more comparable, in this section $q\bar{q} \to \chi\chi^\dagger + j$ is considered instead.

For the reduced mono-jet, the new signal and background cross sections are computed to $\sigma_{q\bar{q}\to\chi\chi^\dagger+X} = (2.3194 \pm 0.0007)$ pb and $\sigma_{q\bar{q}\to\nu\bar{\nu}+X} = (832.8 \pm 0.3)$ pb. These are

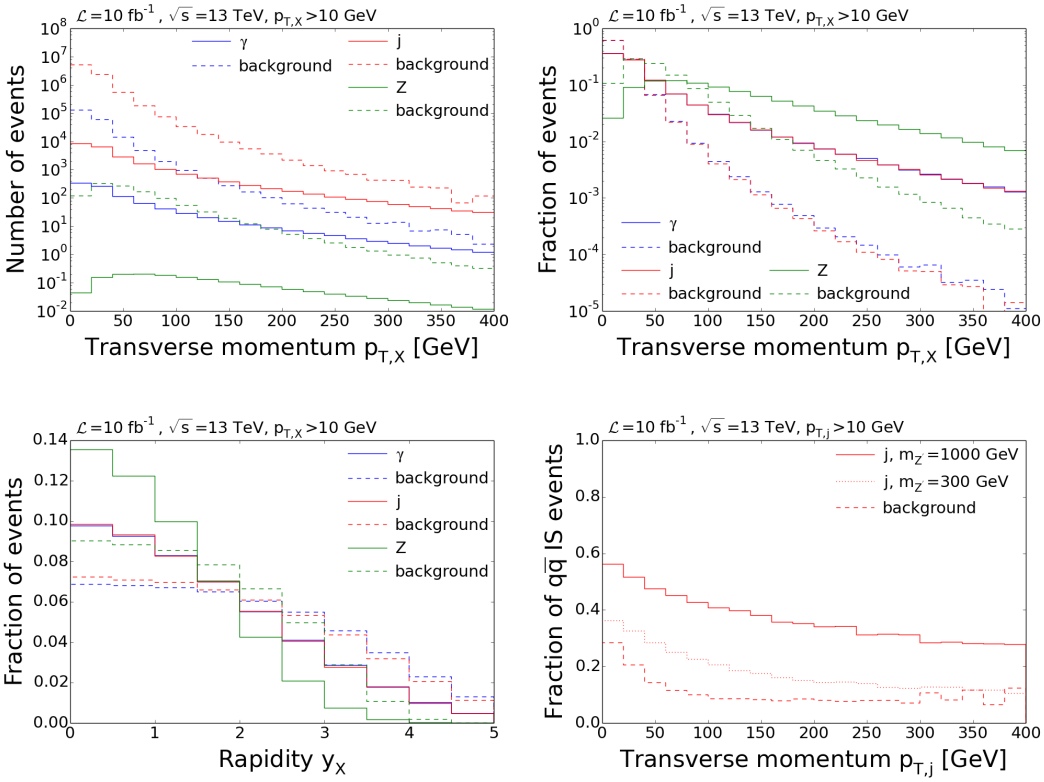

FIG. 4.3: Partonic mono-photon, -Z and -jet events over respective background excluding gluon initial states. Top left: p_T-distributions of all channels of the total rates at $\mathcal{L} = 10$ fb^{-1}. Top right: p_T-distributions of all channels normalised to one. Bottom left: y-distributions of all channels normalised to one. Bottom right: Fraction of $q\bar{q}$ initial states in mono-jet events.

significantly smaller than the full process cross-sections (see Table 4.1).

The same analysis as before is conducted and shown in Fig. 4.3. While the shape of the mono-jet curve in the p_T-regime still looks similar to the full process (see Fig. 4.1), as a result of the decreased cross-section, the absolute rate drops. In the y-plane (see bottom left panel of Fig. 4.3), the mono-jet and mono-photon signals are almost identical. The jet background is radiated more forwardly[2] now. As all jets are completely massless in this case, collineary emission is enhanced. The jet signal is barely affected by this, as the large Z' mass enforces central jet emission, regardless of the the $q\bar{q}/qg$ initial state.

To quantify the effect of the initial state gluons on the signal, the ratios of the calculated rates for signal and background from the processes with and without the gluon are plotted on the bottom right of Fig. 4.3. It can be seen, that for the background this

[2]Forward radiation means that the longitudinal part of the direction of propagation of the scattered particle is dominating. Hence, the scattering angle is rather small. For central radiation, the opposite is the case.

ratio is nearly constant around 0.1 and a little higher for low p_T. Most of the mono-jet background processes have a quark-gluon initial state. The signal consists roughly half of $q\bar{q}$ initial state events and half of events with a quark-gluon initial state. For low p_T, there are slightly more quark-anti-quark initial states, for higher p_T this ratio flips. Excluding the quark-gluon initial state, the jet background decreases by almost an order of magnitude, whereas the jet signal looses about 50 percent. Decreasing the Z' mass to 300 GeV, we see that the ratio becomes lower, meaning the mono-jet process becomes dominated by the quark-gluon initial state. This again can be understood with help of the pdfs. At the Z on-shell production scale of about 90 GeV, the gluon density inside a proton is much higher than at the energy of 1 TeV necessary to produce a Z' on-shell. Thus, the ratio decreases for a lighter Z'.

4.2 Hadronic Signals

So far, we only looked at the bare parton collision processes, producing highly energetic photons, jets or Z's. Due to their high energy though, these particles will decay and collineary radiate off other particles multiple times. This process is called showering and will iterate till the energy dependent QCD coupling is strong enough to bound the decay products and radiated-off particles together into hadrons. This is called hadronization. The resulting final particles are detected in the experiment. In order to make predictions for experimental rates, a detector simulation needs to be included, as detector geometry and properties play a crucial role for the results. PYTHIA [12] is used for simulating parton showering. Detector simulation is done using DELPHES [13] including jet finding and analysis routine FASTJET [14]. We chose to simulate ATLAS, setting the transverse momentum cut for jets to $p^j_{T,min} = 10$ GeV.

In the following, partonic and hadronic (including showering and detector simulation) signals will be compared with each other to examine the differences.

4.2.1 Mono-Jet

In Fig. 4.4, the hadronic mono-jet signal on detector level is compared with the partonic signal. Looking at the total rates in the momentum regime on the top left panel, an increase in signal and background is observed. By that, it can be seen that there are more events than on parton level. This is due to showering, since collinear radiation off the initial state is produced, leading to an increased number of jets. Besides that, the p_T-curves are similar in shape. The little bump in the second bin of the hadronic over the partonic signal is due to the detector internal cut for $p_T > 10$ GeV. Jets that split

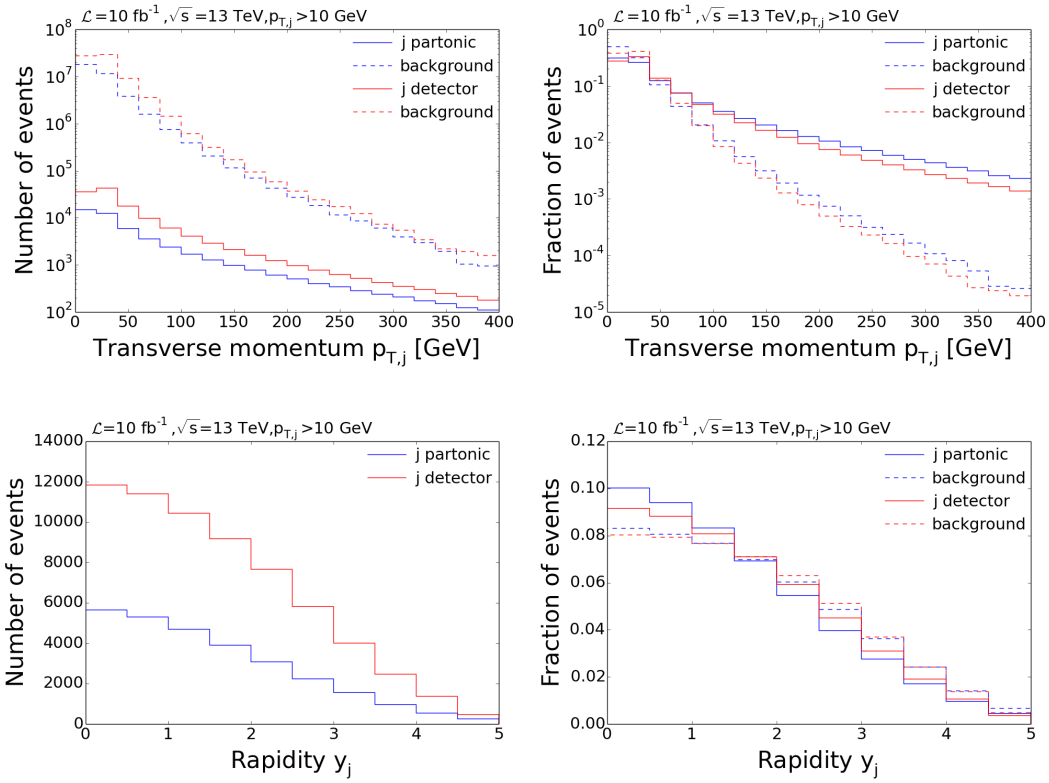

FIG. 4.4: Partonic and hadronic mono-jet events over the respective background. Detector simulation and parton showering are included in the hadronic signal. Top left: p_T-distributions of the total rates at $\mathcal{L} = 10$ fb^{-1}. Top right: p_T-distributions normalized to one. Bottom left: y-distributions at of the total signal rates $\mathcal{L} = 10$ fb^{-1}. Bottom right: y-distributions normalized to one.

while having a transverse momentum slightly above 10 GeV are likely produce at least one jet that is not registered by the detector.

The normalized rates on the top right panel show that the parton jets tend to be slightly harder, for the signal as well as for the background. Generally, it can be seen that the signals are significantly harder than the background. This, as explained before, is caused by the high Z' mass, leading to higher transverse momenta.

Looking at the y-distributions of the partonic and hadronic mono-jet events on the two bottom panels shows, that the signals there behave very similarly. While the event number roughly doubles (left), the shapes are very similar (right). It was omitted to show the total backgrounds over y on the bottom left panel, since, due to the difference in magnitude, the signal shapes would not be discernible as a result of the axis scaling. The same applies to the mono-photon and mono-Z channel.

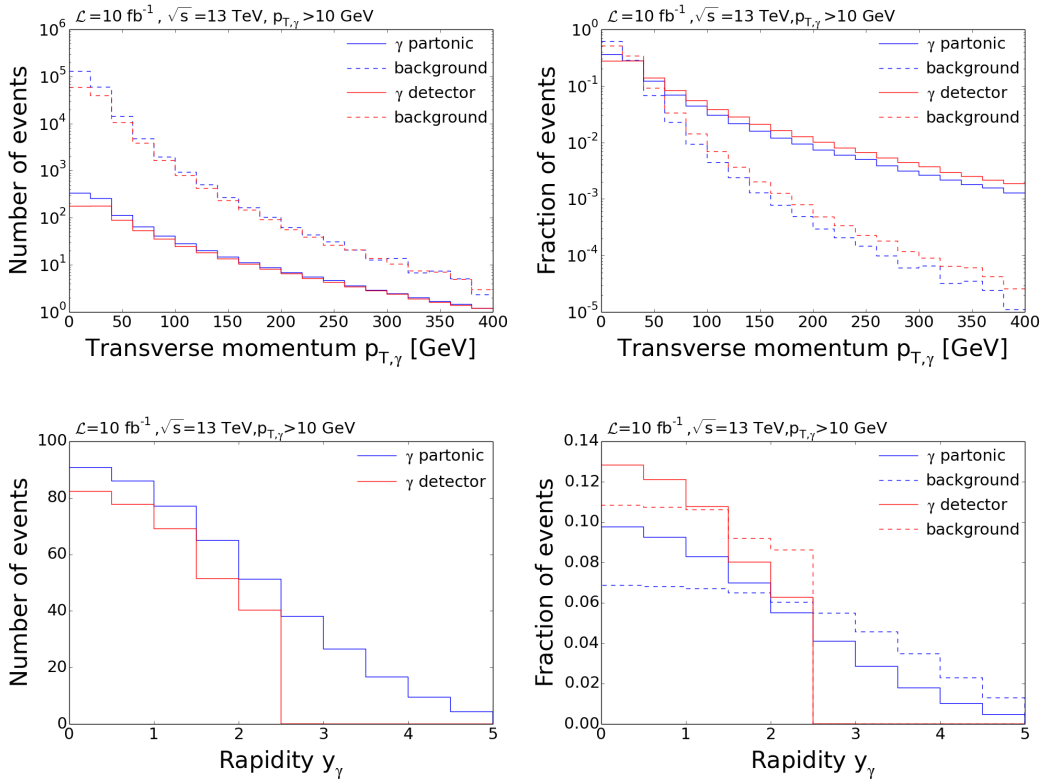

FIG. 4.5: Partonic and hadronic mono-photon events over the respective background. Detector simulation and parton showering are included in the hadronic signal. Top left: p_T-distributions of the total rates at $\mathcal{L} = 10$ fb^{-1}. Top right: p_T-distributions normalized to one. Bottom left: y-distributions of the total signal rates at $\mathcal{L} = 10$ fb^{-1}. Bottom right: y-distributions normalized to one.

4.2.2 Mono-Photon

The mono-photon signature in Fig. 4.5 is barely affected by including showering and detector simulation. The p_T-distributions of the absolute rates (top left panel) are almost identical. The partonic signals have a slight offset in the first two bins compared to the hadronic p_T-curves, which gets even clearer looking at the normalized p_T-distributions on the top right. This is a detector effect. ATLAS does not have sensitivity for photons with $\eta > 2.5$. Since the photons are massless, this cut coincides with the cut on y. This mainly cuts photons with little p_T, as photons in that area are propagating rather forward. Similarly, on hadron level, the photons are slightly harder, as the normalized p_T-distribution shows as well.

In the y-regime, bigger deviations from the parton level curves can be seen (see bottom of Fig. 4.5). The hadronic distributions are cut off for $y > 2.5$. This is due to the detector effect explained above. The hadronic and partonic curves both show that the signals

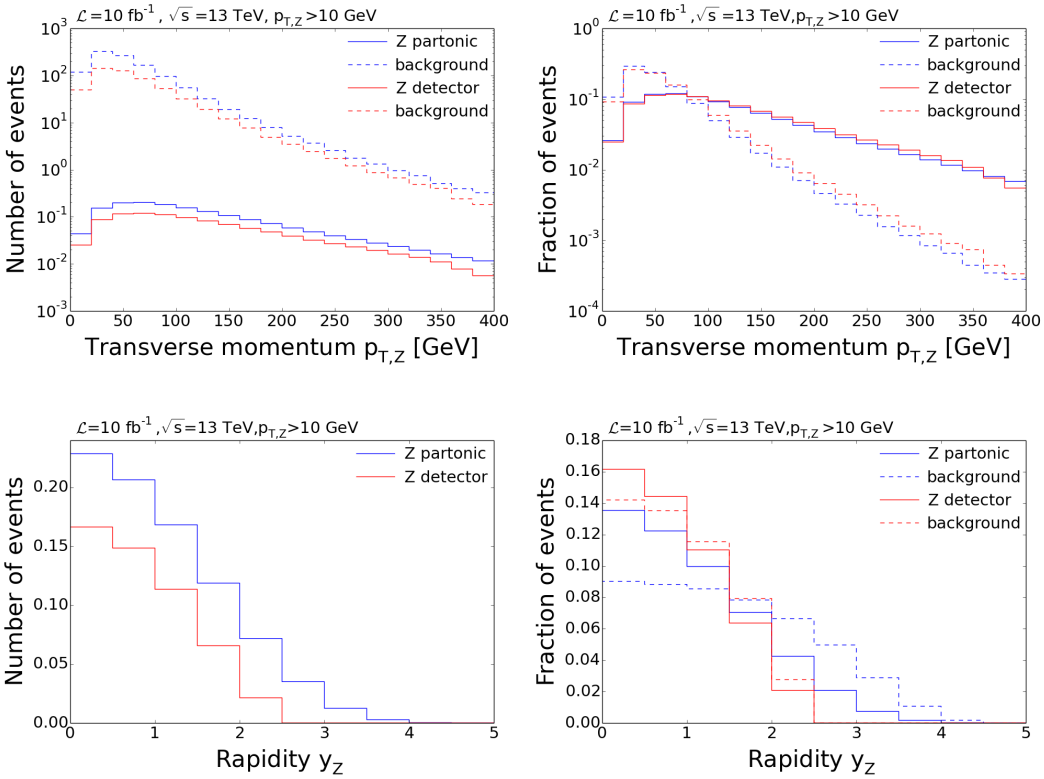

FIG. 4.6: Partonic and hadronic mono-Z events over the respective background. ATLAS detector simulation and parton showering are included in the hadronic signal. Top left: p_T-distributions of the total rates at with $\mathcal{L} = 10$ fb^{-1}. Top right: p_T-distributions normalized to one. Bottom left: y-distributions of the total signal rates at $\mathcal{L} = 10$ fb^{-1}. Bottom right: y-distributions normalized to one.

are scattered more centrally than the mainly forward background. The reason for this, again, lies in the kinematics of the initial state quarks. The background mediator is produced at lower energies, when the q carries most of the energy in the initial $q\bar{q}$ state. As all signals are initial state radiation, the final state photon will be boosted. Its large longitudinal momentum explains why the background is radiated more forwardly. Opposed to that, at the TeV scale, the energy distribution between the $q\bar{q}$ initial state is balanced, meaning there is only little boost of the final state particles. As a result, a more central signal is detected.

4.2.3 Mono-Z

Fig. 4.6 compares the partonic and hadronic signals of the mono-Z channel. The p_T-curves on the top panels have almost identical behaviour on detector and parton level. Only little signal gets lost through showering and detector simulation. The normalized

p_T-distribution on the top right shows that after showering, the resulting muon pairs tend to be a little harder than on parton level.

The y-curves on the bottom right panel show the hadronic events being cut off for $y > 2.5$. The same effect has been observed for the photon in Fig. 4.5. ATLAS has no sensitivity for charged leptons in the regime $\eta > 2.5$. Since the relativistic muons can be treated as massless, we can assume $y_{\mu^\pm} = \eta_{\mu^\pm}$. From kinematic considerations and the additivity of y it now follows that

$$y_Z = \frac{1}{2}\left(y_{\mu^+} + y_{\mu^-}\right). \tag{4.2}$$

Using this, we get

$$y_{\mu^\pm} < 2.5 \Rightarrow y_Z < 2.5.$$

Hence, as a result of the lack of detector sensitivity for leptons with $\eta < 2.5$, the mono-Z rapidity distribution has a cut at 2.5.

Summarizing, in all three channels no big structural differences between the p_T-distributions of the partonic and hadronic signals, including showering and detector simulation, can be seen. While for mono-photon and mono-Z, the normalized distributions show that the hadronic signals tend to be harder, this is not the case for the jet. Further, the number of mono-jet events increases as a result of the parton shower (see Fig. 4.4).

Comparing the y-distributions on parton and hadron level, it becomes clear that detector effects play a big role. The observed differences between parton and hadron level are dominated by ATLAS lacking sensitivity for $\eta > 2.5$.

4.2.4 Detector Level Results

In Fig. 4.7 the final signals of mono-photon, mono-jet and mono-Z events, as they are registered in the detector, are compared. The total rates are still by far biggest for the mono-jet channel. Mono-Z is still the signature with the lowest rates. At $\mathcal{L} = 10$ fb^{-1}, the signal curve does not surpass one event per bin. The signal shapes of all signatures in the p_T-regime are very similar to parton level (see Fig. 4.1).

Furthermore, a deviations between the three channels in the final y-distributions can be seen. In the detector, the mono-jet channel looks different from mono-Z and mono-photon. The detector effects responsible for this were discussed previously. However, it has to be taken into account that in the y plane, we are comparing distributions normalized after all cuts. The heights of the curves, relative to each other, do not say anything

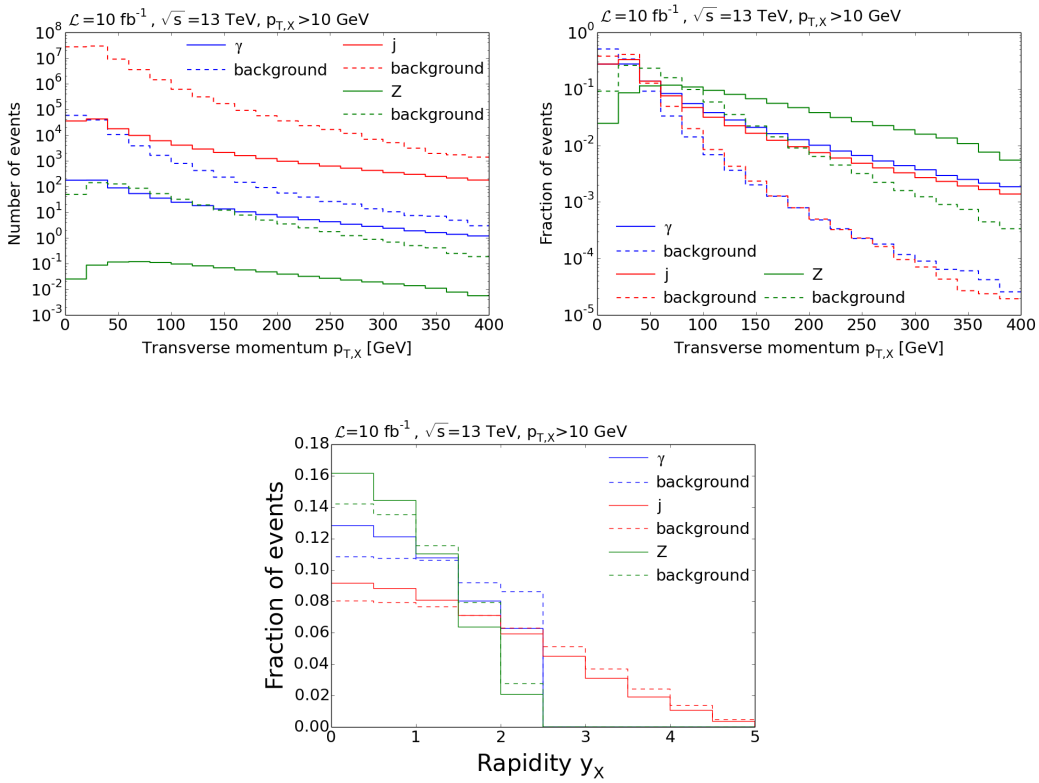

FIG. 4.7: Hadronic mono-photon, -Z and -jet events over respective background at $\sqrt{s} = 13$ TeV including parton shower and detector simulation. Top left: p_T-distributions of the total rates at $\mathcal{L} = 10$ fb^{-1}. Top right: p_T-distributions normalized to one. Bottom: y-distribution normalized to one.

about the relative signal strengths. Only the respective signals and backgrounds are comparable to each other. As we are rather interested in signal shapes, this normalization is sufficient. The structural differences between the detector level signals become clear. It was shown in the previous analysis, that considering absolute rates, mono-jet is the strongest channel.

In Fig. 4.8 the p_T- and y-distribution of the three different channels are plotted once more, now applying a realistic detector cut onto the transverse momentum of $p_T > 100$ GeV. From the two top panels showing the total and normalized p_T-distributions, it can be seen that in this momentum region, all three signal look very alike. The shapes are almost identical. As the cut excludes mainly the forwardly radiated particles, only the shape of the mono-jet's y-distributions on the bottom panel significantly changes. The curve is not as flat anymore, but as a result of the cut steeper and vanishing for $y > 4$, so for very little scattering angles. Mono-photon and mono-Z are barely affected, due

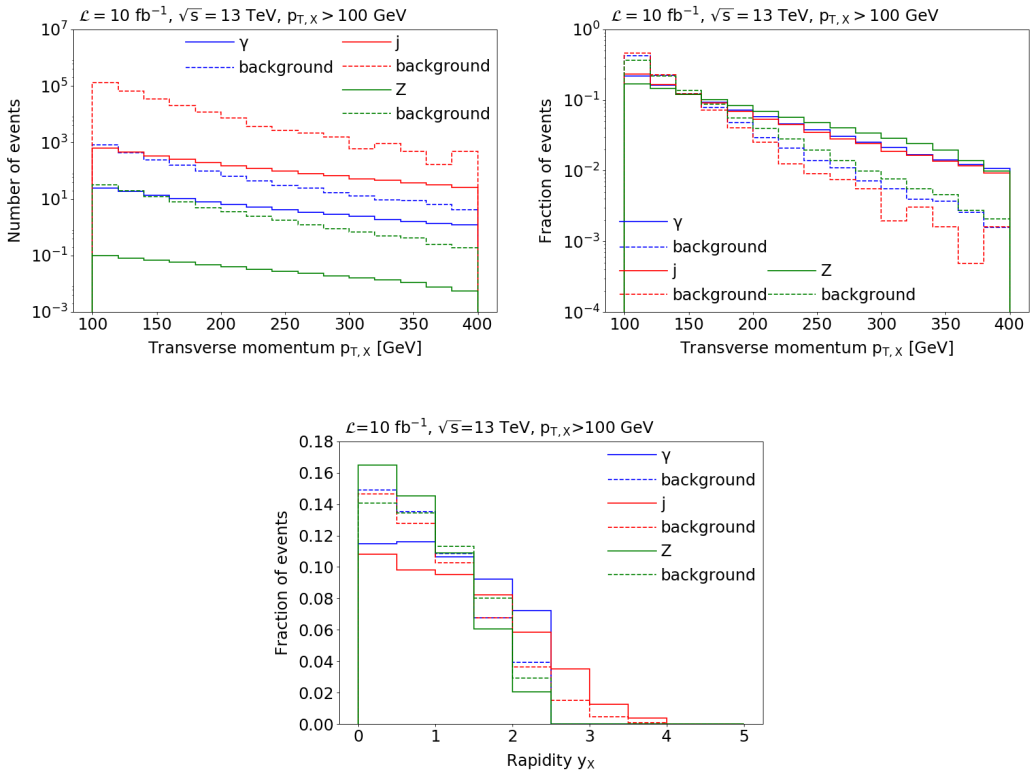

FIG. 4.8: Hadronic mono-photon, -Z and -jet events over respective background with $p_{T,X} > 100$ GeV at $\sqrt{s} = 13$ TeV including parton shower and detector simulation. Top left: p_T-distributions of the total rates at $\mathcal{L} = 10$ fb^{-1}. Top right: p_T-distributions normalized to one. Bottom: y-distributions normalized to one.

the lack of detector sensitivity for these two channels in the forward direction.

It can be concluded, that, including parton showering and detector simulation, the results obtained just from the bare partonic processes (see Fig. 4.1), are confirmed. The difference in signal strength between the photon and jet signals gets even bigger after showering and running the detector simulation. The mono-Z channel still is much weaker by several orders of magnitude. Applying a realistic detector cut of $p_T > 100$ GeV, the signals of the different channels show very similar shapes in the p_T and y-regime. Hence, what really distinguishes them are the total event rates of signals and backgrounds. Looking at the significances of the different channels, it gets clear than in an experimental scenario, the mono-jet channel has very strong advantages over the other two signatures, assuming models that feature DM signals in form of ISR.

5 Conclusions and Outlook

In this work, a simplified model was used to describe DM pair production through a heavy Z' boson decaying into complex scalar DM particles. In this framework, simulations of proton-proton collisions, as they are happening at the LHC, were ran and rates for DM signals of the form $X + \not{E}_T$ were predicted. X was considered to be either a jet, photon or a Z-boson decaying into muons. It was observed that the mono-jet channel gives by far higher rates than mono-photon or mono-Z signatures, resulting in a much higher LHC sensitivity. This is quantified by the detector level significances for the respective channels, shown in Fig. 5.1 as a function of p_T cuts. Each bin as a width of 20 GeV. For mono-jet, the significance on hadron level including showering and detector simulation is quite constant, decreasing towards higher p_T. The mono-photon channel's significance is smaller by a factor two, showing less sensitivity to this signature. The significances of the mono-Z signature are much smaller than one. It gets clear, that jet is strongly dominating. Applying a realistic experimental p_T-cut at around 100 GeV, the mono-jet channel surpasses the other two signatures in every momentum region. The strong advantage of the mono-jet channel in experimental scenarios gets very clear.

However, we did not intend to make solid statements about absolute collider sensitivities. Rather than the absolute positions of the significance curves in Fig. 5.1, the relative positions matter and underline our conclusion. To achieve meaningful results for absolute LHC sensitivities, this study needs to be carried out cautiously in terms of the exact parameter choices, as the parameter space and the DM production cross-sections of the studied scenarios are strongly constrained by direct detection experiments.

Furthermore, this work included a detailed kinematic analysis of the studied processes. By looking at the $p_{T,X}$- and η_X-distributions of the different channels, it became clear, that the mono-jet and mono-photon signatures have a very similar kinematic structure. For the mono-Z channel, differences due to the high Z mass could be observed. Furthermore, from the analysis of the mono-Z processes, it could be understood how $m_{Z'}$ influences the kinematics of these kind of collision processes, especially in the y-plane. We were able to relate many kinematic features to the parton density functions of the ini-

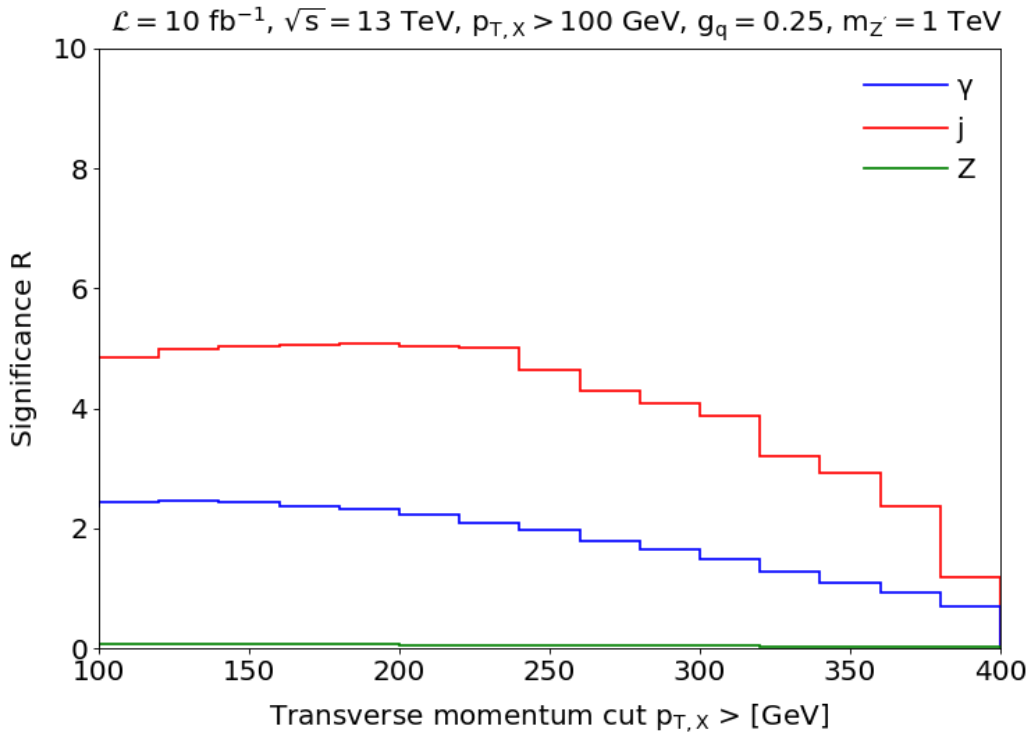

FIG. 5.1: Significances of hadronic mono-jet, -photon and -Z events at $\sqrt{s} = 13$ TeV and $\mathcal{L} = 10$ fb^{-1} including parton showering and detector simulation.

tial state particles. Detector effects dominate the deviations between hadron and parton level events. Applying realistic detector cuts, the signals resemble each other strongly with little differences in the direction of emission. Hence, the signal and background strengths are crucial for collider sensitivity, strongly favouring mono-jet searches, as it gets clear by Fig. 5.1.

It follows, that in the framework of simplified models, where signals arise as ISR, mono-jet searches will always yield an advantage compared to mono-photon and mono-Z searches. The ratios of the different channels' signals only depend on the SM vertices where X is radiated off the initial state particles. Here, the difference in coupling strength will always favour mono-jet over mono-photon and mono-Z. The mono-Z channel is additionally suppressed by the high Z mass. Thus, our conclusions concerning the relative collider sensitivities are independent of the dark interaction and are not influenced by χ being fermionic or scalar, heavier or lighter. Hence, in mono-photon and mono-Z searches, this branch of models is not very promising, as mono-jet searches are

much more likely to detect at signal from ISR scenarios.

A strong signal improvement for the mono-Z signature can be achieved by underlying a Minimal Supersymmetric Model (MSSM). Modelling DM to be the lightest neutralino, one can produce a final state Z resonantly. This can lead to significantly higher cross-sections. Future research will be carried out on these type of models.

6 Acknowledgements

This thesis would have never become what it is without the strong support of many friends, colleagues and those who are and became both. The first person I want to thank is my supervisor Prof. Dr. Tilman Plehn. He always had his door open for me and gave me the opportunity and time to learn and understand many, many new things about physics. Further, I thank Jun.-Prof. Dr. Susanne Westhoff, who contributed to my work with her expertise and a lot of helpful advice.

I would like to acknowledge Dr. Martin Bauer for his patience and time, dedicatedly teaching and explaining physics to me. To Dr. Nikolai Zerf, I want to say thank you for the many coffee QFT lectures and wisdoms.

I am very grateful for the enormous help of Anja Butter, who advised me and put a lot of thought into this project. Likewise, it is a great pleasure to thank Dr. Torben Schell and Johann Bremer, for being there for me with any smallest question. Furthermore, I thank Elias Bernreuther for continuing this project and the laughs we shared. Also, I want to express my gratitude to all the other members of the LHC pheno group. I had a great time with you and enjoyed every single day in this group.

Last but not least, I want to say thank you to my dear friends involved in this thesis: Stefan Blücher for the uncountable coffee and lunch times, always being there to keep me from working just at the right times, and Thorben Frank and Moritz von Schwartzenberg for their thorough proof-reading and valuable input.

Bibliography

[1] NASA. `https://map.gsfc.nasa.gov/universe/bb_tests_cmb.html`. Accessed: 2017-03-06.

[2] P. A. R. Ade et al. Planck 2015 results. XIII. Cosmological parameters. *Astron. Astrophys.*, 594:A13, 2016.

[3] Tilman Plehn. Dark matter from a particle theorists perspective. `http://www.thphys.uni-heidelberg.de/~plehn/pics/dark_matter.pdf`. Accessed: 2017-03-21.

[4] Nadav Priel. XENON100 Results on WIMP and non-WIMP Searches. In *Proceedings, 10th Patras Workshop on Axions, WIMPs and WISPs (AXION-WIMP 2014): Geneva, Switzerland, June 29-July 4, 2014*, pages 37–40, 2014.

[5] Teresa Marrodn Undagoitia and Ludwig Rauch. Dark matter direct-detection experiments. *J. Phys.*, G43(1):013001, 2016.

[6] Ringaile Placakyte. Parton Distribution Functions. In *Proceedings, 31st International Conference on Physics in collisions (PIC 2011): Vancouver, Canada, August 28-September 1, 2011*, 2011.

[7] Tilman Plehn. *Lectures on LHC Physics*, volume 886. 2015.

[8] Daniele Alves. Simplified Models for LHC New Physics Searches. *J. Phys.*, G39:105005, 2012.

[9] Adam Alloul, Neil D. Christensen, Cline Degrande, Claude Duhr, and Benjamin Fuks. FeynRules 2.0 - A complete toolbox for tree-level phenomenology. *Comput. Phys. Commun.*, 185:2250–2300, 2014.

[10] Johan Alwall, Michel Herquet, Fabio Maltoni, Olivier Mattelaer, and Tim Stelzer. MadGraph 5 : Going Beyond. *JHEP*, 06:128, 2011.

[11] Eric Conte, Benjamin Fuks, and Guillaume Serret. MadAnalysis 5, A User-Friendly Framework for Collider Phenomenology. *Comput. Phys. Commun.*, 184:222–256, 2013.

[12] Torbjorn Sjostrand, Stephen Mrenna, and Peter Z. Skands. PYTHIA 6.4 Physics and Manual. *JHEP*, 05:026, 2006.

[13] J. de Favereau, C. Delaere, P. Demin, A. Giammanco, V. Lematre, A. Mertens, and M. Selvaggi. DELPHES 3, A modular framework for fast simulation of a generic collider experiment. *JHEP*, 02:057, 2014.

[14] Matteo Cacciari, Gavin P. Salam, and Gregory Soyez. FastJet User Manual. *Eur. Phys. J.*, C72:1896, 2012.

Declaration

I assure, that I wrote this thesis independently and did not use any other than the stated sources and means.

Heidelberg, the 27th of March 2017

Jan Horak